

UNCLASSIFIED  
~~CONFIDENTIAL~~

Copy 6  
RM E54G20

NACA RM E54G20

# NACA

## RESEARCH MEMORANDUM

INVESTIGATION OF THREE HIGHLY LOADED SUBSONIC-INLET-  
STAGE AXIAL-FLOW COMPRESSORS EMPLOYING VARYING  
RADIAL GRADIENTS OF ENERGY ADDITION

By Raymond M. Standahar

Lewis Flight Propulsion Laboratory  
Cleveland, Ohio

CLASSIFIED DOCUMENT

This material contains information affecting the National Defense of the United States within the meaning of the espionage laws, Title 18, U.S.C., Secs. 793 and 794, the transmission or revelation of which in any manner to an unauthorized person is prohibited by law.

### NATIONAL ADVISORY COMMITTEE FOR AERONAUTICS

WASHINGTON

October 25, 1954

*MAILED*  
*7/17/58*  
*1958*  
by authority of *RA-129* *5/1/58* Date *7/17/58*

CLASSIFICATION CHANGED

~~UNCLASSIFIED~~

~~CONFIDENTIAL~~

UNCLASSIFIED



## NATIONAL ADVISORY COMMITTEE FOR AERONAUTICS

RESEARCH MEMORANDUMINVESTIGATION OF THREE HIGHLY LOADED SUBSONIC-INLET-STAGE AXIAL-FLOW  
COMPRESSORS EMPLOYING VARYING RADIAL GRADIENTS OF ENERGY ADDITION

By Raymond M. Standahar

## SUMMARY

Three axial-flow-compressor inlet stages having a hub-tip diameter ratio of 0.5 were investigated to determine: (1) whether high pressure ratios can be obtained by means of high turning with highly cambered subsonic types of blading, and (2) the effectiveness of radial gradients of energy addition in reducing the deceleration across the rotor tip and thus relieving the effect of high tip loading.

A stage designated A, consisting of guide vanes, rotor and stator, was assigned a constant value of dimensionless energy addition of approximately 0.4 over the entire blade span. The design values of pressure ratio and maximum relative inlet Mach number were 1.59 and 0.80, respectively. Designs B and C were designed for the same tip loading as design A but used a medium and large gradient of energy addition, respectively, from the hub to the tip blade section. The pressure ratios for designs B and C were 1.42 and 1.39, respectively.

A maximum over-all efficiency of 0.66 and an over-all pressure ratio of 1.35 was reached at design speed for design A. For design B, the over-all adiabatic efficiency was approximately 0.90 and the over-all pressure ratio was 1.40. The over-all adiabatic efficiency and pressure ratio for design C were 0.89 and 1.36, respectively.

The rotor-tip section for each design was in a state of continuous stall and, as a result, vibration severely limited the operating range of each design. Tip blade stall was undoubtedly due to the high rate of diffusion at this section (as measured by D factor) and, therefore, the blade-element data against diffusion factor are also presented.

There was a large radial shift in flow downstream of the rotor and stator and as a result, the radial distribution of efficiency measured past the rotor of each design varied greatly from that past the stator.

Although the integrated results for designs B and C appeared to be good, the outlet-flow distribution varied greatly from the design value, and the staging of a compressor using these stages would be very difficult.

## INTRODUCTION

For design-speed operation of an inlet stage, the principal requirements are high weight flow per unit frontal area, high wheel speed, and high stage pressure ratio at an acceptable efficiency. Studies of multi-stage axial-flow compressors (ref. 1) have indicated that, in order to obtain efficient off-design performance, it is necessary for the inlet stage to operate efficiently over wide equivalent-speed and weight-flow ranges. Although cascade data indicated that the range of efficient angle of attack decreased as the camber was increased, there was no available compressor data using high cambers.

As part of the general program to obtain design limitations for axial-flow compressors, three single-stage units were built using design values of energy addition that were well above the values normally used for subsonic-type blading. The purpose of this investigation was to determine if high pressure ratios in an inlet stage could be obtained by the use of large turning angles with highly cambered blades, instead of using high rotor relative inlet Mach numbers.

A stage (design A) was designed with an approximately constant value of  $\Delta H/U_t^2$  (dimensionless enthalpy addition) of 0.4 over the entire blade length. Since this led to very high blade cambers at the hub, designs B and C employed a medium and large gradient of energy addition from the tip to the hub blade section, which decreased the diffusion across the blade and permitted blades of lower camber to be used near the hub. All three rotors were of the subsonic type using NACA 65-series variable camber blades and were designed for an inlet relative Mach number limit of 0.8 and the same tip energy addition. For the rotor designated A, the theoretical free-stream lift coefficient varied from 3.0 at the hub to 2.3 at the tip; design B varied from 1.5 at the hub to 2.5 at the tip; and design C varied from 0.92 at the hub to 2.0 at the tip.

The three single-stage compressors were investigated over a range of speeds and weight flows.

## SYMBOLS

The following symbols were used in this report:

- |            |   |
|------------|---|
| $C_L$      | camber (lift coefficient of isolated airfoil)                                     |
| D          | diffusion factor  |
| $\Delta H$ | enthalpy rise, $\text{ft}^2/\text{sec}^2$   |
| h          | dimensionless ratio of axial component of air velocity to tip speed,<br>$V_z/U_t$ |

M	Mach number
P	absolute stagnation or total pressure, lb/sq ft
p	static pressure, lb/sq ft
r	radius, ft
T	stagnation temperature, °R
U	wheel speed, ft/sec
V	absolute air velocity, ft/sec
w	weight flow, lb/sec
$\frac{w\sqrt{\theta}}{\delta}$	weight flow corrected to NACA standard sea-level pressure and temperature, lb/sec
x	ratio of tangential velocity to tip speed, $V_{\theta}/U_t$
z	radius ratio, $r/r'_t$
$\alpha$	angle of attack, deg
$\gamma$	ratio of specific heats
$\delta$	ratio of inlet stagnation pressure to NACA standard sea-level pressure, $P_0/2116$
$\eta$	adiabatic temperature-rise efficiency
$\theta$	ratio of inlet stagnation temperature to NACA standard sea-level temperature, $T_0/518.6$
$\mu$	blade setting angle, deg
$\rho$	air density, slug/cu ft
$\sigma$	solidity, ratio of chord length to distance between adjacent blades

## Subscripts:

ad	adiabatic
av	average
h	hub
t	tip
z	axial direction

- $\theta$  tangential direction
- 0 depression tank
- 1 upstream of rotor
- 2 downstream of rotor
- 3 downstream of stator

Superscript:

- ' relative to rotor

### COMPRESSOR DESIGN

The three single-stage compressor designs investigated were tested in the same variable-component axial-flow test rig. The designs were based on the following assumptions:

- (1) Constant tip radius  $r_t$  of 7 inches
- (2) Simple radial equilibrium of pressure and no radial flow  
( $1/\rho \, dp/dr = v_\theta^2/r$ )
- (3) Rotor efficiency of 0.90 with no area allowance for flow blockage due to boundary layer
- (4) Rotor relative Mach number limit  $M_1'$  equal to approximately 0.80
- (5) Hub-tip diameter ratio of 0.5 at the rotor leading edge

Design A was a constant total enthalpy design with a value of  $\Delta H/U_t^2$  equal to approximately 0.40 for the entire blade span. As this particular design was based on cylindrical flow, the value of  $\Delta H/U_t^2$  at the hub would be 0.425, based on the actual hub contour. A symmetrical velocity diagram at all radii and a relative inlet-air angle of  $60^\circ$  was used at the rotor tip. The design values of pressure ratio and rotor tip speed were 1.59 and 1052 feet per second, respectively. Design weight flow was 28.08 pounds per second, which corresponds to 26.2 pounds per square foot of frontal area.

To relieve the blade loading at the hub in design B, the energy addition  $\Delta H/U_t^2$  was reduced linearly from a value of 0.40 at the tip to a value of 0.25 at the hub section, based on estimated streamline flow. This resulted in design values for pressure ratio and tip speed of 1.42

and 1072 feet per second, respectively. The weight flow was 28.12 pounds per second or 26.3 pounds per square foot of frontal area.

In design C, the energy addition  $\Delta H/U_t^2$  at the hub was further reduced to a value of 0.175. This reduction gave more relief to the blade loading and lowered the design pressure ratio to 1.39. Values of weight flow per square foot of rotor frontal area and tip speed were 26.1 and 1072 feet per second, respectively. Design C was also based on estimated streamline flow.

The values necessary to construct the design velocity diagrams for the three designs are given in figure 1. The guide vanes for all three designs were 0.060-inch-thick sheet-metal blades having a circular-arc camber line. The guide vanes were designed on the basis of references 2 and 3. The type of loading used in design A resulted in an unusual type of guide vane in that the guide-vane angles were positive at the tip and negative at the hub. The required turning was obtained by varying the chord length as well as the radius of curvature of the blade. For designs B and C, the guide vanes had a constant radius of curvature, and the variation of turning was obtained by varying the chord length. The guide-vane geometry for all three designs is presented in table I.

The rotor and stator blades were all of NACA 65-series compressor blades. Table II gives the blade geometry for all the rotor and stator blades. The cascade data available at the time of design did not present values of camber greater than 2.7 at a solidity of 1, or 2.4 at a solidity of 1.5. Therefore, the cascade data were extrapolated to obtain the higher lift coefficients used in these designs. A plot of design values of diffusion factor (ref. 4) for all three designs is presented in figure 2 to show the range of design diffusion factor covered. As shown in figure 2, the design rotor D factor is above 0.4 for nearly the entire range, while the tip section is never below a value of 0.7. The design stator D factors for the three designs are also lowered, as shown in figure 2. The values of stator D factor range from a nearly constant value of 0.7 for design A to a minimum value of 0.4 for design B and 0.2 for design C.

#### APPARATUS AND PROCEDURE

Test facility. - A schematic diagram of the compressor installation is shown in figure 3. The compressor was driven by a 1500-horsepower motor through a speed-increasing gear box. Atmospheric air was drawn through a thin plate orifice, and then into a 6-foot-diameter depression tank. Filter paper and a series of screens were installed in the tank to obtain uniform flow into the bell-mouth inlet of the compressor. The desired inlet pressure was set by means of a remotely controlled valve at the entrance to the depression tank. The air was discharged from the compressor collector into the laboratory exhaust system. A valve in the outlet duct controlled the air flow.

Instrumentation. - Air flow into the compressor was measured by means of a thin plate orifice. The pressure drop, in inches of water, across the orifice was measured by means of a micromanometer. The temperature at the orifice was measured by four iron-constantan thermocouples located just ahead of the orifice. Inlet tank temperature and pressure were measured by five iron-constantan thermocouple probes and five wall static-pressure taps spaced around the tank circumference (fig. 3, station 0). The depth of immersion of the thermocouples was such that measurements were made at the centers of equal annular areas. Because of the large tank diameter and consequent low air velocity, measured values of temperature and pressure were assumed equal to stagnation conditions for calculation of compressor performance.

Circumferential surveys were taken downstream of the inlet guide vanes (fig. 4, station 1) to locate the wake regions, and thereafter, measurements at all radii of total pressure, flow angle, and static pressure were taken between blade wakes. This measuring station was approximately  $1/2$  inch ahead of the rotor. Wall static-pressure taps were also provided at the inner and outer walls. The total temperature at this station was assumed to be equal to the depression-tank total temperature. Station 2 was located about  $1/4$  inch behind the rotor blades. Station 3 was located  $1\frac{1}{2}$  inches downstream of the stator blades. Four static-pressure taps were located on both the inner and outer walls of the annular flow passage at both stations. There were also provisions for taking radial and circumferential surveys of total pressure, flow angle, static pressure, and total temperature. The location of the measuring stations is indicated in figure 4. Data were taken at five radial stations, which were located at the centers of five equal-area increments across the annular passage at the various axial stations.

Table III presents the number of probes and type of instruments used at each measuring station. Figure 5 shows photographs of the various probes used during the investigation of design A. During the tests of design B, it was found necessary to take circumferential surveys downstream of the rotor and stator because of the wide circumferential variations of the flow that were measured. This method of operation became very time-consuming and, as a result, a recording device was devised for the last series of tests whereby the total pressure, temperature, and flow angle were plotted against probe position as the various probes were moved circumferentially across the passage. To insure that the temperature probe was correctly aligned with the flow, a thermocouple was combined with a directional probe, as shown in figure 5(e).

The static-pressure and thermocouple probes used in this investigation were calibrated over the range of Mach numbers obtained in these tests.

The total-pressure loss across the guide vanes was obtained at each radial measuring station for several weight flows by means of circumferential wake surveys of total pressure. This loss for a given weight flow

was then subtracted from the depression-tank total pressure to give the total pressure downstream of the guide vanes.

The mass-averaged total-pressure ratio was obtained from the following equation:

$$\left(\frac{P_3}{P_0}\right)_{av} = \left\{ \frac{\int_{r_{h,3}}^{r_t} \left[ \left(\frac{P_3}{P_0}\right)^{\frac{\gamma-1}{\gamma}} - 1 \right] \rho_3 V_{z,3} r_3 dr}{\int_{r_{h,3}}^{r_t} \rho_3 V_{z,3} r_3 dr} + 1 \right\}^{\frac{\gamma}{\gamma-1}}$$

The average adiabatic temperature-rise efficiency was calculated from a mass-flow weighted average of the total-temperature rise across the rotor and a mass-flow weighted average of the isentropic power input as

$$\eta_{ad} = \frac{\int_{r_{h,3}}^{r_t} T_0 \left[ \left(\frac{P_3}{P_0}\right)^{\frac{\gamma-1}{\gamma}} - 1 \right] \rho_3 V_{z,3} r_3 dr}{\int_{r_{h,3}}^{r_t} (T_3 - T_0) \rho_3 V_{z,3} r_3 dr}$$

The diffusion factor D (ref. 4) was calculated by means of the following equation:

$$D = \left( 1 - \frac{V_2'}{V_1'} \right) + \frac{\Delta V_1'}{2\sigma V_1'}$$

Test procedure. - The performance of all three inlet stages was investigated over a range of air flows at rotor speeds corresponding to 50, 75, and 100 percent of design speed. At each speed, the depression-tank air pressure was held at 25 inches of mercury absolute. The air flow at each speed was varied from the maximum flow obtainable to a flow where surge or excessive rig vibration was encountered. In testing design A, the flow was lowered to a point where the flow angle after the guide vanes was noticeably affected by the severe tip stall of the rotor. This particular set of blades failed after approximately 70 hours of operation, probably as a result of the vibration caused by operating with a continuous tip stall. Because of this failure, the other two blade designs were not operated as far into the stall region.

## RESULTS AND DISCUSSION

Over-all stage performance. - Figure 6(a) is a plot of over-all mass-averaged adiabatic efficiency and pressure ratio against corrected weight flow for design A. A maximum efficiency of 0.66 and an over-all pressure ratio of approximately 1.35 was reached during the design speed run which covered a range of about  $5\frac{1}{2}$  pounds of corrected weight flow. This compressor stage did not have an audible surge, but the rotor tip section was continuously in a state of stall, and severe rig vibration finally became the limiting factor in the range.

Over-all adiabatic efficiency and pressure ratio against corrected weight flow are presented in figure 6(b) for design B. At design speed, a maximum efficiency of approximately 0.90 and an over-all pressure ratio of 1.40 were reached. Although the hub position was afforded some relief by a drop in work input, it did not alleviate the stall condition at the tip, and the tests were curtailed because of severe rig vibration. Because of the fatigue failure of the first set of blades due to blade vibration, these tests were not carried far into the vibration region, and as a result, the indicated range is only 1 pound of corrected weight flow at design speed.

As shown in figure 6(c), design C, which had a larger gradient of energy addition from hub to tip than either of the two previous designs, gave an over-all adiabatic efficiency of 0.89 and a total-pressure ratio of 1.36. Here again, because of the high design energy addition at the tip section, a stall condition severely limited the operating range of this stage to 1 pound of corrected weight flow at design speed.

Diffusion factor. - The D factors for five radial elements of the rotor were calculated and are presented against adiabatic efficiency for the three designs in figure 7. The data of reference 4 indicate that, for a tip region efficiency of 0.90, D factors should be no greater than 0.45, and for the mean radius and hub positions, a rapid rise in loss factor occurs at D factors greater than 0.6. In all three cases reported herein, the tip position D factor is greater than 0.75 and the tip-element efficiencies are below 0.70. All the D factors of design A are above 0.55 and the corresponding efficiencies are less than 0.80. A point of interest here is that the efficiencies seem to drop rapidly at a D factor value of approximately 0.6. In design B, the D factors drop down to a low of 0.4 and the corresponding efficiencies increase to a maximum value of approximately 0.93 at the hub. As shown in reference 5, it is possible for the low-energy air near the hub to be centrifuged out to the tip position, and as a result, the hub element efficiencies may not include all the actual losses associated with that particular radial element. The measured efficiencies of the lower radial positions for design C increased slightly from the value obtained for design B to a maximum value of 0.95. This slight increase in efficiency may be due to the fact that the D factors for design C are slightly lower than the D factors for design B, and as a result, the blades are not as highly loaded. Although the measured

diffusion factor at the rotor tip is above 0.75 for all three designs (fig. 7), and the corresponding tip-element efficiencies never exceed 0.70, the integrated over-all efficiencies (figs. 6(b) and (c)) of designs B and C are around 0.89, while that of design A (fig. 6(a)) is down to 0.66. This would indicate that high loading at the rotor tip can be tolerated insofar as integrated over-all performance is concerned, as long as the lower sections of the blade are afforded some relief in loading. For these designs, however, the rotor tip is always in a state of stall, and as a result, a large radial shift in flow causes the stators to operate far from their design points.

Because of the radial flow and tip-stall condition in addition to the very low temperature rise at low speed, it was impossible to obtain consistent elemental efficiencies for the stage at 50 and 75 percent of design speed. For this reason, the element performance for design speed only is presented.

Element performance. - The element efficiencies measured at design speed downstream of the rotor and stator are plotted against corrected weight flow in figure 8 for all three designs. These plots show that the efficiencies downstream of the rotor do not follow the same radial pattern as those of the complete stage. For design A (fig. 8(a)), the efficiency at radial position b downstream of the rotor is much below the values for the other radial positions for the major portion of the flow range. The efficiency of the hub section is the highest of all the sections for the entire flow range. This distribution of efficiency is probably due to the fact that the outer portion of the blade is stalled and, as mentioned previously, the low-energy air at the hub is being carried out to the tip along the blade, thereby causing the indicated efficiencies at the lower sections of the blade to appear high.

The efficiencies of the hub section downstream of the stator for design A have dropped down to values equal to or below the efficiency values of the tip section. Here again, this low efficiency indication is probably caused by the low-energy air being carried down to the hub of the stator blade, as shown in reference 5.

In design B (fig. 8(b)), the rotor tip efficiency is still poor, but the efficiency of radial position b has improved markedly. As the tip section has the same measured loading as design A, this improvement in the performance of sections a and b can be attributed to the fact that the blade loading at the other sections has been reduced. As a result of this unloading, it is probable that less low-energy air is being centrifuged to the outer radial positions. Also, the reduction in axial velocity across the rotor tip section is decreased, thereby reducing some of the losses associated with large surface velocity diffusion. This improvement in rotor performance is also reflected in the fact that the element efficiencies downstream of the stator are generally higher than those of design A.

The element efficiencies of design C (fig. 8(c)) follow the same pattern as those of design B, probably because the loading at the hub for design B was below the critical value and further reduction in loading at this station did not tend to improve the performance appreciably. Since the general level of efficiency for design A was much lower than for designs B and C, some thought was given to the possibility of the reverse-turning inlet guide vanes disturbing the inlet flow distribution. The guide vanes for design A had a reversal of turning from tip to hub, while the guide vanes for designs B and C were of a proven design turning in one direction. Figure 9 is therefore presented to compare the design guide-vane turning for design A with the actual turning obtained. The measured guide-vane turning agreed with that of design, and as a result, the guide-vane performance is not believed to be a contributing cause of the poor performance of this design.

Another possible reason for these low tip efficiencies is the magnitude of the rotor relative inlet Mach number. The relative inlet Mach numbers for each of the three designs is presented in table IV. These Mach numbers are all at or above the point where the total-pressure loss coefficient starts to increase rapidly for a 65-(12)10 blade section (ref. 6). As most of these blade sections have design lift coefficients greater than 1.2, it would be expected that the loss coefficients for these sections would start to increase at lower values of Mach number. This comparison of relative inlet Mach numbers for all three designs, however, would tend to eliminate Mach number as a main source of the extremely poor performance of design A, since the range of Mach number shown in table IV covers approximately the same values for all three designs.

Stage discharge flow distribution. - The measured flow angles and axial velocities downstream of the stator blades are compared with the design values for all three designs in figure 10. In design A, the leaving angles ranged from  $4^\circ$  above design at the tip measuring station to approximately  $10^\circ$  lower than design at the hub measuring station. The measured axial velocity downstream of the stators is greater than the design values at all radii. This large increase in the axial velocities is a direct result of the stage pressure ratio and efficiency being much lower than design. The outlet flow distributions for designs B and C follow the same general trend in that the flow angles are higher than design near the tip section and lower than design at the hub section. The measured leaving axial velocity for design B is much higher than design at the hub and decreases in value to approximately design value at the tip. The leaving axial velocity for design C is also higher than design at the hub but decreases to a value below design at the tip. Since the measured outlet flow distribution varies greatly from the design values for all three designs, the staging of these designs would be very difficult.

## SUMMARY OF RESULTS

The following results were obtained with three single-stage inlet-type axial-flow compressors designed for varying amounts of energy addition. A stage designated as A was assigned a constant value of dimensionless energy addition of approximately 0.4 over the entire blade span. The design values of pressure ratio and maximum relative inlet Mach number were 1.59 and 0.80, respectively. Designs B and C were designed for the same tip loading as design A but used a medium and large gradient of energy addition, respectively, from the hub to the tip blade section. The pressure ratios for designs B and C were 1.42 and 1.39, respectively.

1. At the design tip speed of 1052 feet per second for design A, a peak pressure ratio of 1.35 and an adiabatic efficiency of 0.66 were reached at a corrected weight flow of 26.7 pounds per second (25.0 lb/(sec)(sq ft of frontal area)).

2. A peak pressure ratio of 1.40 and an efficiency of 0.90 for a tip speed of 1072 feet per second were obtained for design B at a corrected weight flow of 28 pounds per second (26.2 lb/(sec)(sq ft of frontal area)).

3. At design tip speed of 1072 feet per second for design C, a peak pressure ratio of 1.36 and an adiabatic efficiency of 0.89 were obtained at a corrected weight flow of 27.7 pounds per second (25.9 lb/(sec)(sq ft of frontal area)).

4. The measured diffusion factor at the rotor tip for all three designs was above 0.75 and the corresponding element efficiencies were all below 0.70.

5. High blade loading at the rotor tip did not seem to result in low over-all integrated efficiency, as long as the lower sections of the blade were afforded some relief in loading.

6. Since the measured outlet flow distribution varies greatly from the design values for all three designs, the staging of these designs would be very difficult.

Lewis Flight Propulsion Laboratory  
National Advisory Committee for Aeronautics  
Cleveland, Ohio, July 15, 1954

CK-2 back

## REFERENCES

1. Finger, Harold B., and Dugan, James F., Jr.: Analysis of Stage Matching and Off-Design Performance of Multistage Axial-Flow Compressor. NACA RM E52D07, 1952.
2. Lieblein, Seymour: Turning-Angle Design Rules for Constant-Thickness Circular-Arc Inlet Guide Vanes in Axial Annular Flow. NACA TN 2179, 1950.
3. Lieblein, Seymour, and Ackley, Richard H.: Secondary Flows in Annular Cascades and Effects on Flow in Inlet Guide Vanes. NACA RM E51G27, 1951.
4. Lieblein, Seymour, Schwenk, Francis C., and Broderick, Robert L.: Diffusion Factor for Estimating Losses and Limiting Blade Loadings in Axial-Flow-Compressor Blade Elements. NACA RM E53D01, 1953.
5. Rohlik, Harold E., Allen, Hubert W., and Herzig, Howard Z.: Study of Secondary-Flow Patterns in an Annular Cascade of Turbine Nozzle Blades with Vortex Design. NACA TN 2909, 1953.
6. Briggs, William B.: Effect of Mach Number on the Flow and Application of Compressibility Corrections in a Two-Dimensional Subsonic-Transonic Compressor Cascade Having Varied Porous-Wall Suction at the Blade Tips. NACA TN 2649, 1952.

TABLE I. - GUIDE-VANE GEOMETRY

Design	Radial position	Blade camber angle, deg	Blade chord, in.	Solidity	Radius of curvature, in.
A	Hub	-26.0	1.63	2.22	3.6
	Mean	16.2	1.18	1.06	4.2
	Tip	60.3	2.3	1.57	2.3
B	Hub	6.2	0.27	0.35	2.3
	Mean	27.8	1.11	1.00	↓
	Tip	54.6	2.15	1.47	↓
C	Hub	10.7	0.44	0.60	2.3
	Mean	20.8	1.14	1.04	↓
	Tip	55.0	2.17	1.48	↓

TABLE II. - BLADE DESIGN VALUES

[Chord length of all blades, 1.83 in.; rotor blade thickness, from 6 percent at tip to 10 percent at radius ratio of 0.5; stator blade thickness, 10 percent.]

Rotor					Stator				
Radius ratio, z	Solidity, $\sigma$	Camber, $C_L$	Angle of attack, $\alpha$ , deg	Blade setting angle, $\mu$ , deg	Radius ratio, z	Solidity, $\sigma$	Camber, $C_L$	Angle of attack, $\alpha$ , deg	Blade setting angle, $\mu$ , deg
Design A									
0.50	1.67	3.00	34.0	14.0	0.50	2.00	3.00	38.5	13.5
.60	1.39	2.90	29.7	18.5	.60	1.67	2.80	32.5	18.8
.70	1.19	2.74	26.3	23.5	.70	1.43	2.60	27.5	25.0
.75	1.12	2.65	24.6	26.5	.75	1.33	2.50	25.4	28.2
.80	1.04	2.57	23.1	29.7	.80	1.25	2.40	23.5	32.0
.90	.93	2.40	20.2	38.0	.90	1.11	2.20	20.7	41.0
1.00	.83	2.30	18.2	53.0	1.00	1.00	2.10	19.0	57.0
Design B									
0.522	1.59	1.52	19.1	22.9	0.577	1.73	1.50	19.8	25.4
.615	1.35	1.62	18.3	26.3	.657	1.52	1.35	16.9	30.3
.711	1.17	1.73	17.8	30.2	.740	1.35	1.24	15.0	34.9
.807	1.02	1.84	17.2	35.0	.825	1.21	1.17	13.6	39.7
.904	.92	1.92	17.0	40.5	.912	1.05	1.14	12.6	45.1
1.000	.83	2.49	20.2	47.7	1.000	1.00	1.06	11.4	55.3
Design C									
0.522	1.59	0.92	13.3	24.9	0.577	1.73	0.52	10.2	31.9
.615	1.35	1.18	14.4	28.1	.657	1.52	.56	9.9	35.2
.711	1.17	1.42	15.3	31.5	.740	1.35	.58	9.2	38.9
.807	1.02	1.64	15.8	35.7	.825	1.21	.58	8.9	42.8
.904	.92	1.78	16.1	40.6	.912	1.05	.58	8.2	47.6
1.000	.83	2.03	17.0	46.2	1.000	1.00	.58	7.8	53.2

TABLE III. - INSTRUMENTS

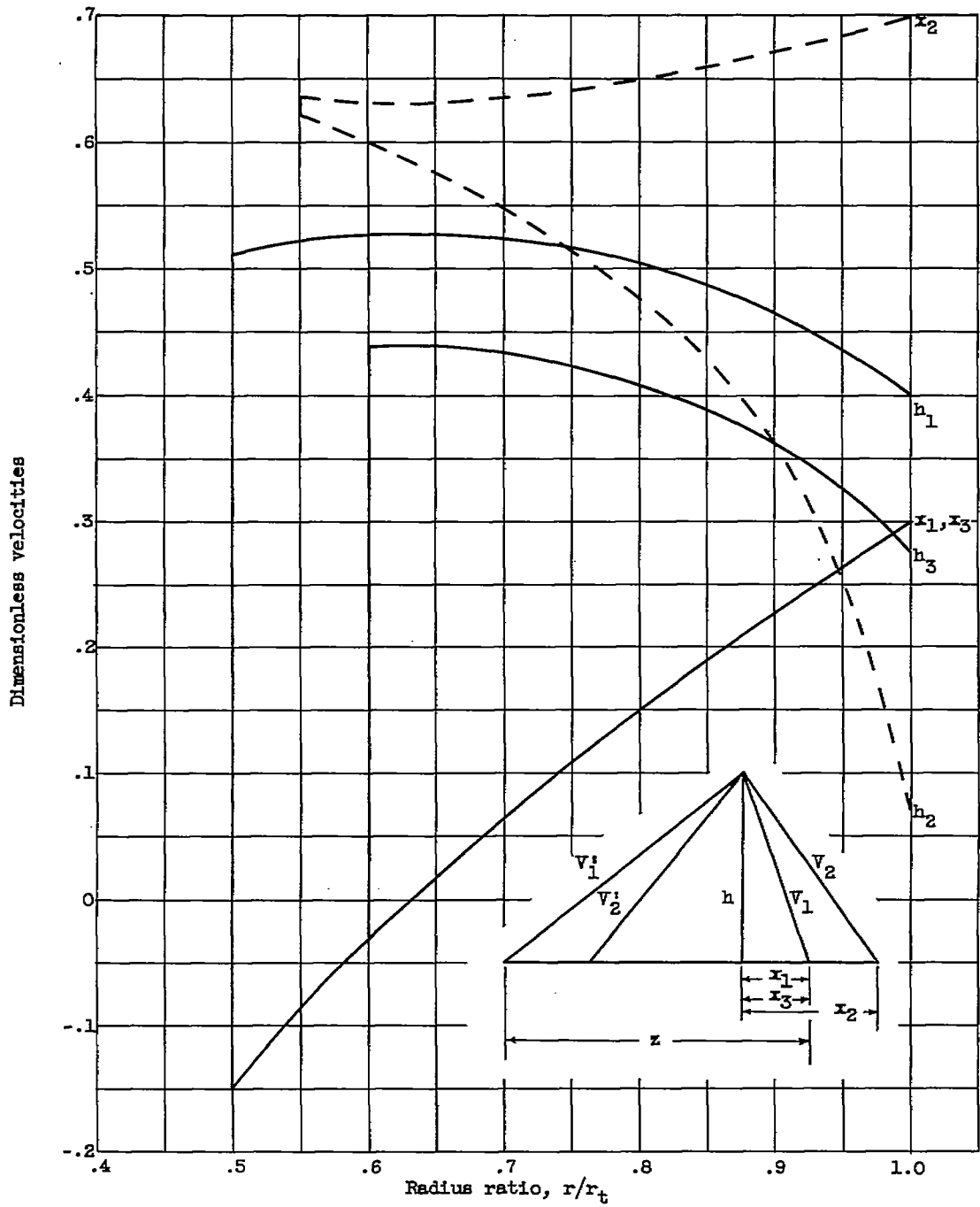
Station	Temperature	Stagnation pressure	Static pressure	Angle
Inlet orifice	Four iron-constantan thermocouples	Barometer reading	Two wall static-pressure taps	
Depression tank	Five iron-constantan thermocouples		Five wall static-pressure taps	
Downstream of guide vanes		$P_1 = P_0$ minus guide-vane losses	One wedge-type static-pressure probe <sup>a</sup>	One claw total-pressure type yaw measuring probe <sup>b</sup>
Downstream of rotor 2	Self-balancing spike-type thermocouple <sup>c</sup>		Four wall taps	One claw total-pressure type yaw measuring probe
Design A				
Downstream of stator 3	Four 5-tip double stagnation-type temperature rakes <sup>d</sup>	Five 19-tube stagnation-pressure rakes <sup>e</sup>	Four wall taps, one wedge-type static-pressure probe	One claw total-pressure type yaw measuring probe
Designs B - C				
3	Self-balancing spike-type thermocouple <sup>c</sup>	Claw total-pressure type	Four wall taps, one wedge-type static-pressure probe	One claw total-pressure type yaw measuring probe

<sup>a</sup>Fig. 5(a).<sup>b</sup>Fig. 5(b):<sup>c</sup>Fig. 5(e).<sup>d</sup>Fig. 5(c).<sup>e</sup>Fig. 5(d).

TABLE IV. - ROTOR RELATIVE INLET MACH NUMBER

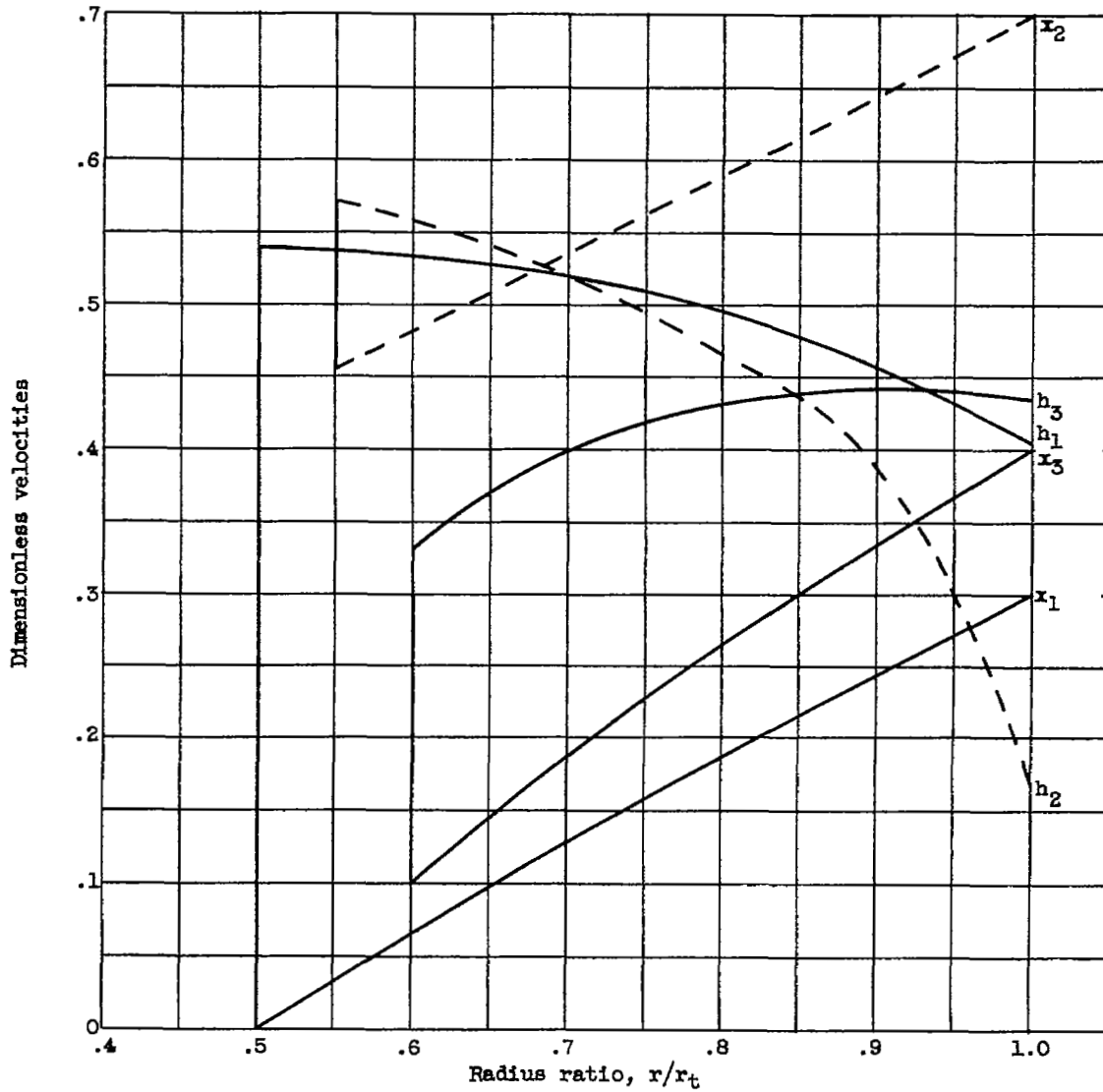
		Design A	Design B	Design C
Design value of $M'$	Hub	0.80	0.73	0.68
	Tip	.77	.80	.80
Calculated value of $M'$ at design speed	Hub	0.75 to 0.78	0.76 to 0.78	0.74 to 0.77
	Mean	0.81 to 0.84	0.79 to 0.82	0.77 to 0.80
	Tip	0.79 to 0.81	0.78 to 0.81	0.78 to 0.81

3335  
OK-3



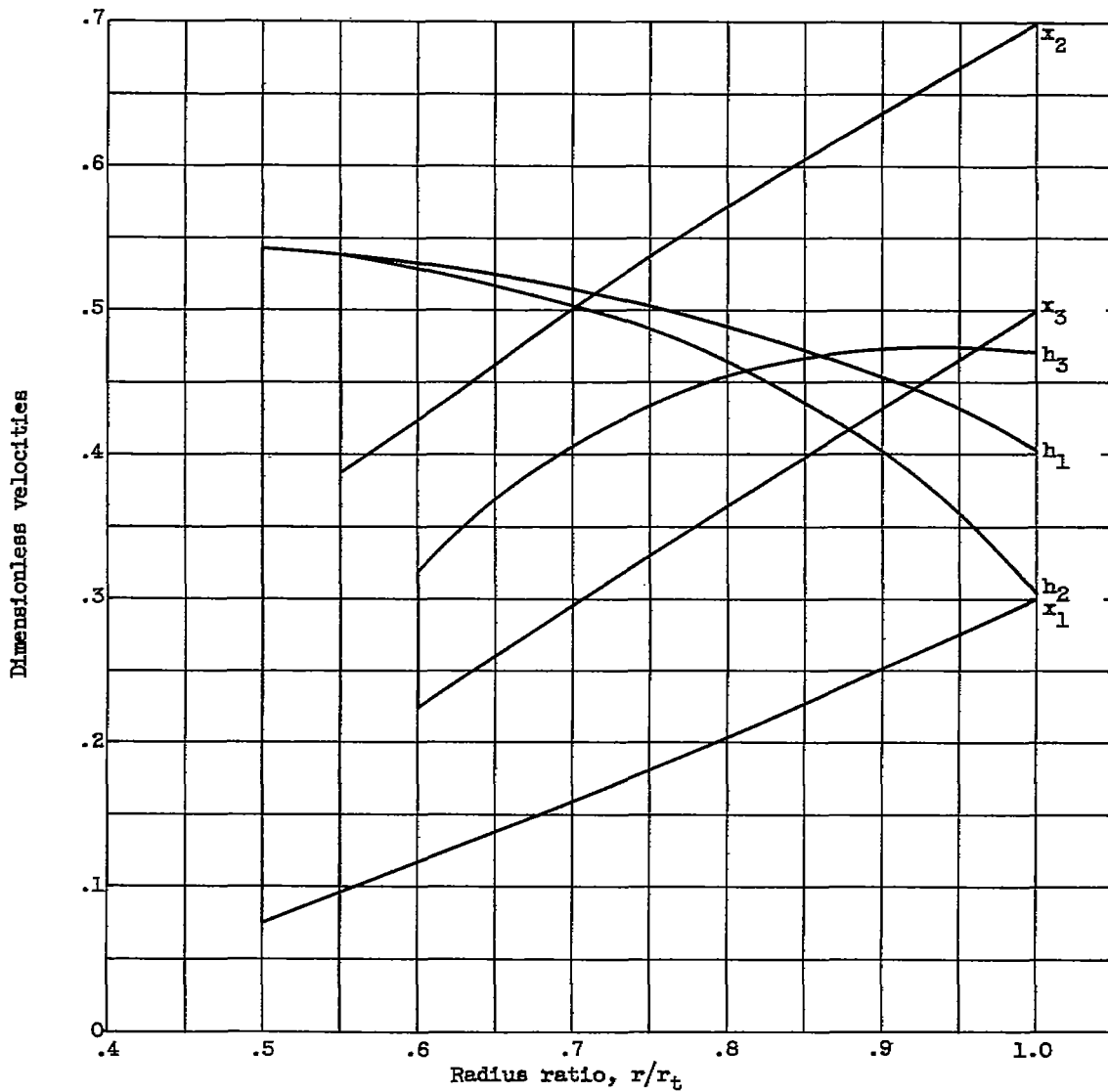
(a) Design A. Weight flow, 28.08 pounds per second; tip speed, 1052 feet per second.

Figure 1. - Design velocity ratios.



(b) Design B. Weight flow, 28.12 pounds per second; tip speed, 1012 feet per second.

Figure 1. - Continued. Design velocity ratios.



(c) Design C. Weight flow, 27.89 pounds per second; tip speed, 1072 feet per second.

Figure 1. - Concluded. Design velocity ratios.

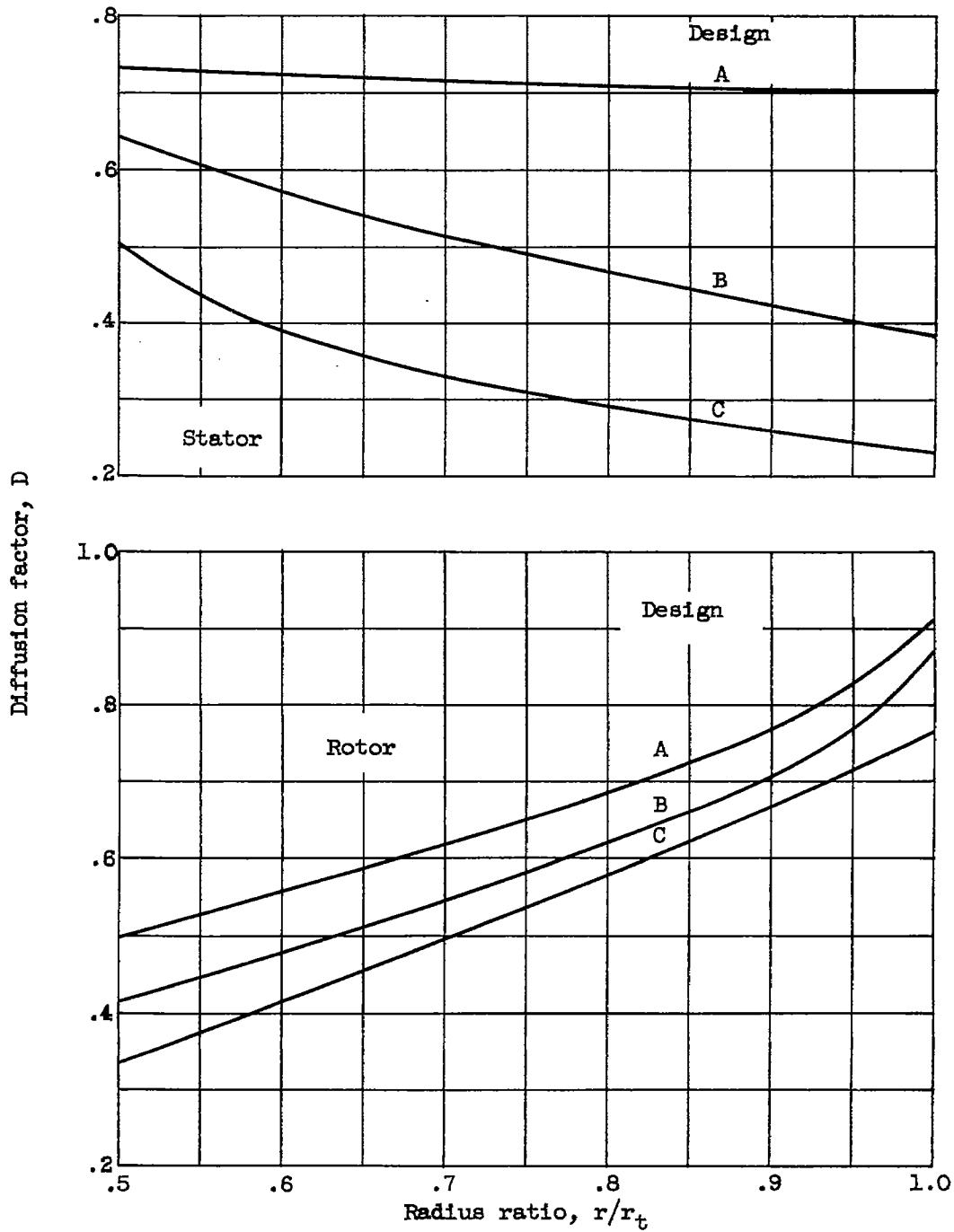


Figure 2. - Design values of diffusion factor for rotor and stator of all three designs.

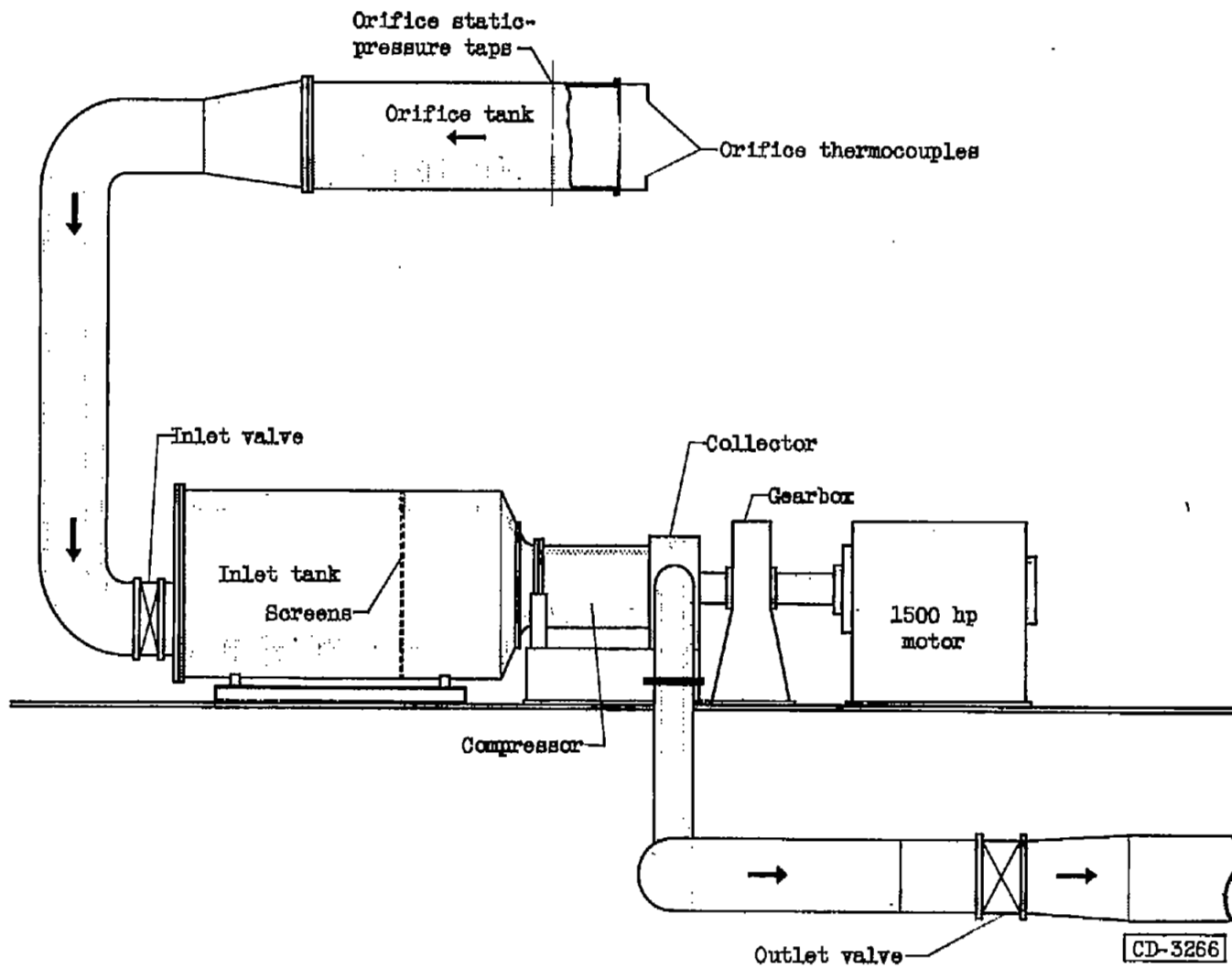


Figure 3. - Compressor installation.

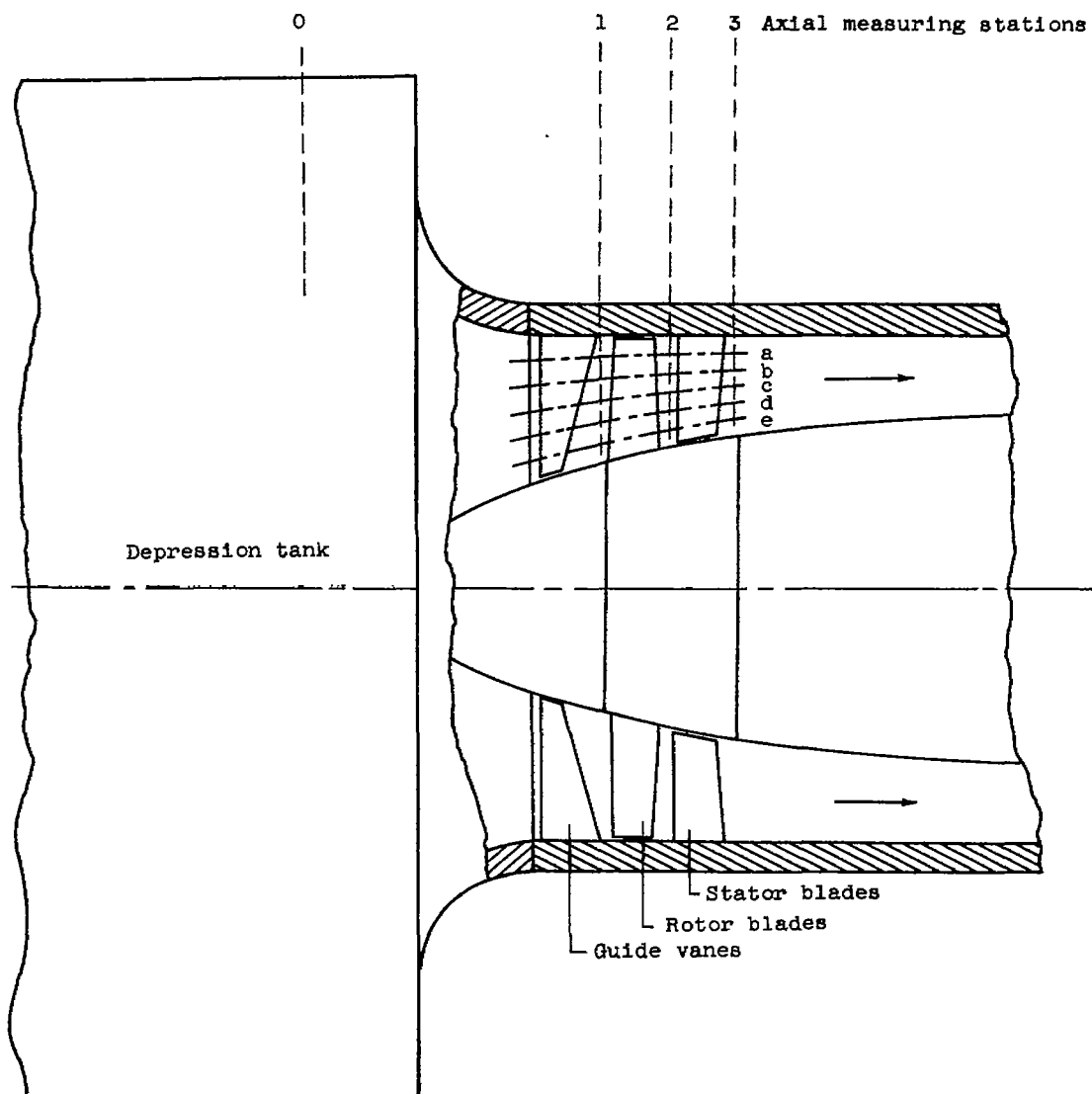
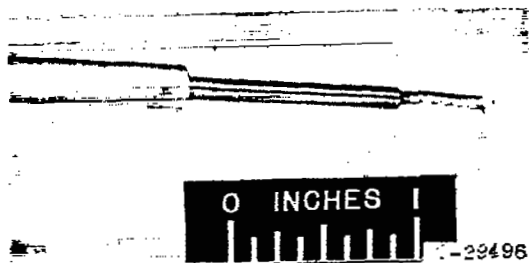
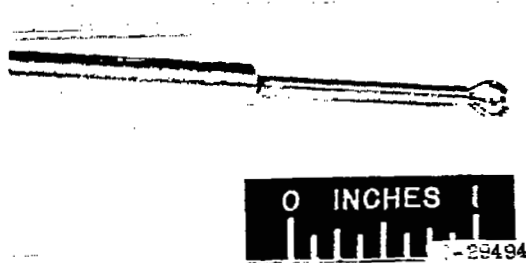


Figure 4. - Instrumentation stations.

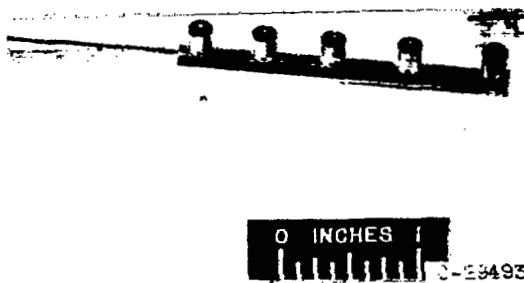
3335



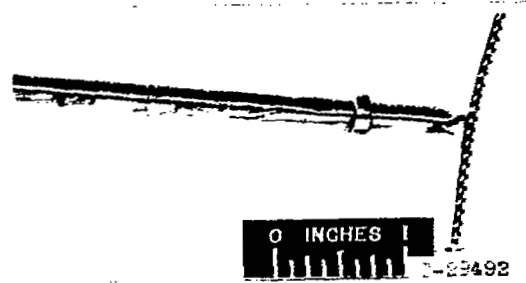
(a) Static-pressure wedge.



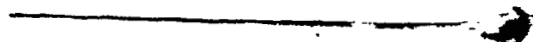
(b) Claw total-pressure-type yaw measuring probe.



(c) Double stagnation-type thermocouple probe.

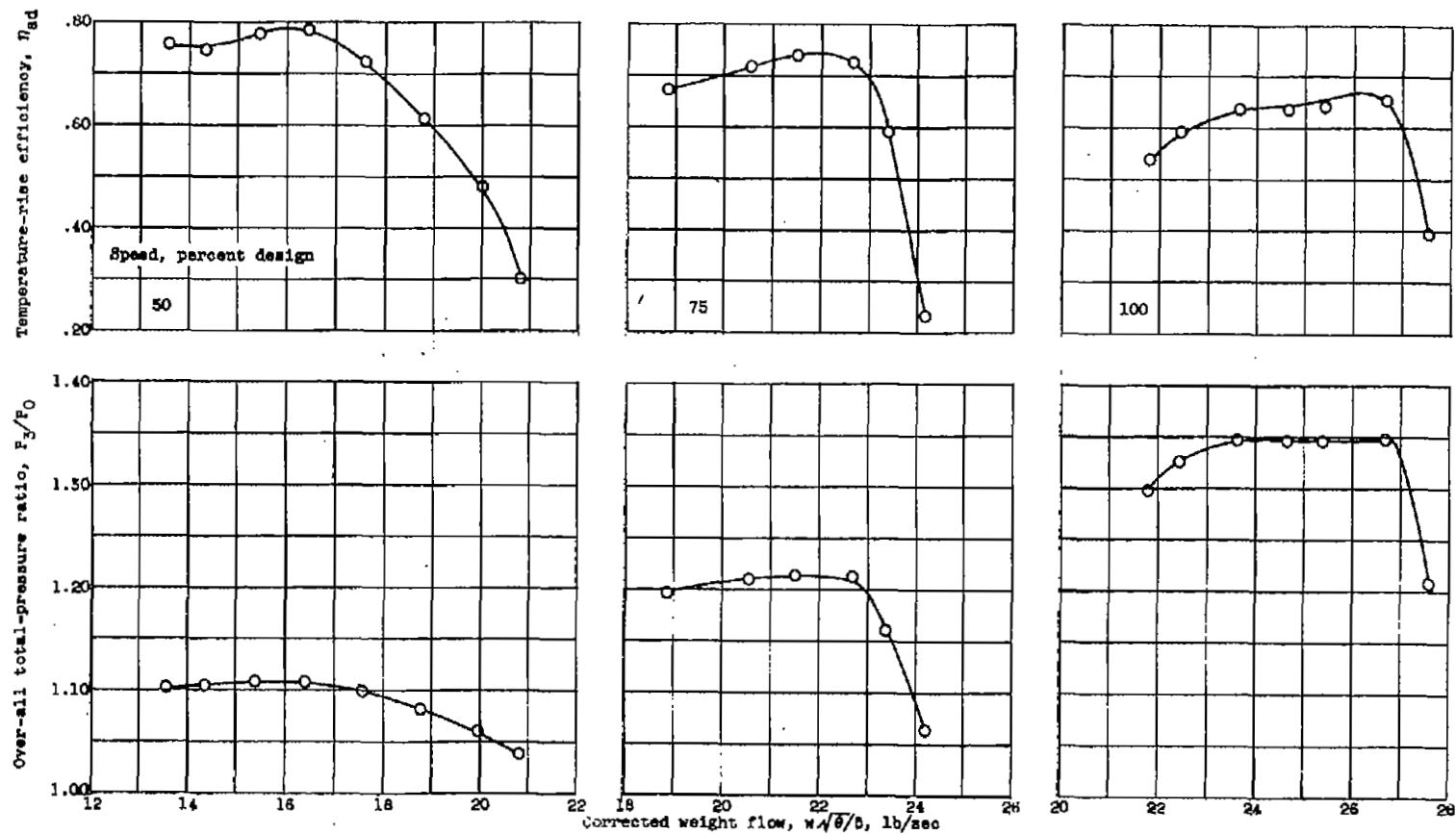


(d) Total-pressure rake.



(e) Spike-type thermocouple.

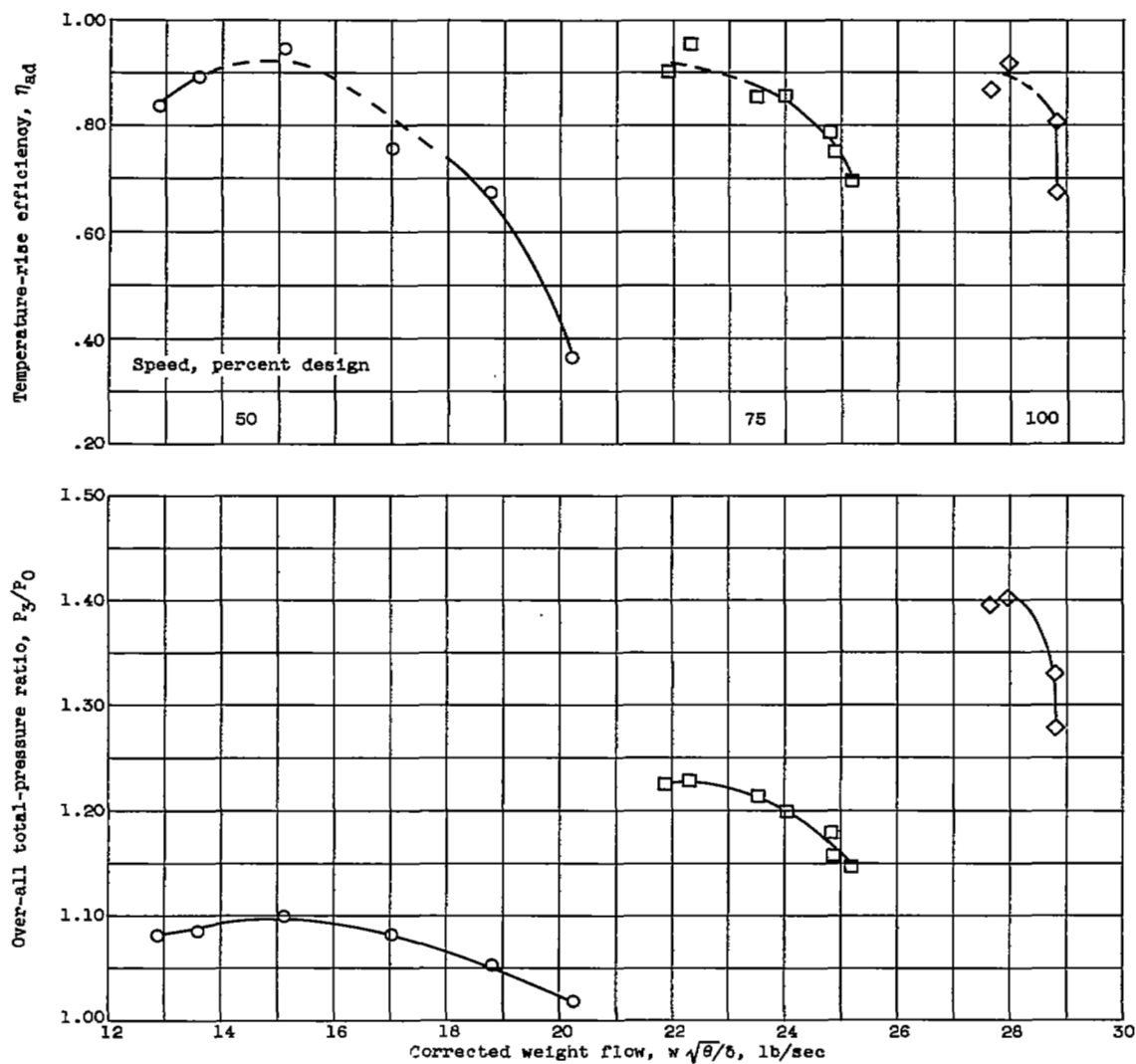
Figure 5. - Instruments.



(a) Design A.

Figure 6. - Variation of over-all total-pressure ratio and temperature-rise efficiency with corrected weight flow.

CK-4 3335



(b) Design B.

Figure 6. - Continued. Variation of over-all total-pressure ratio and temperature-rise efficiency with corrected weight flow.

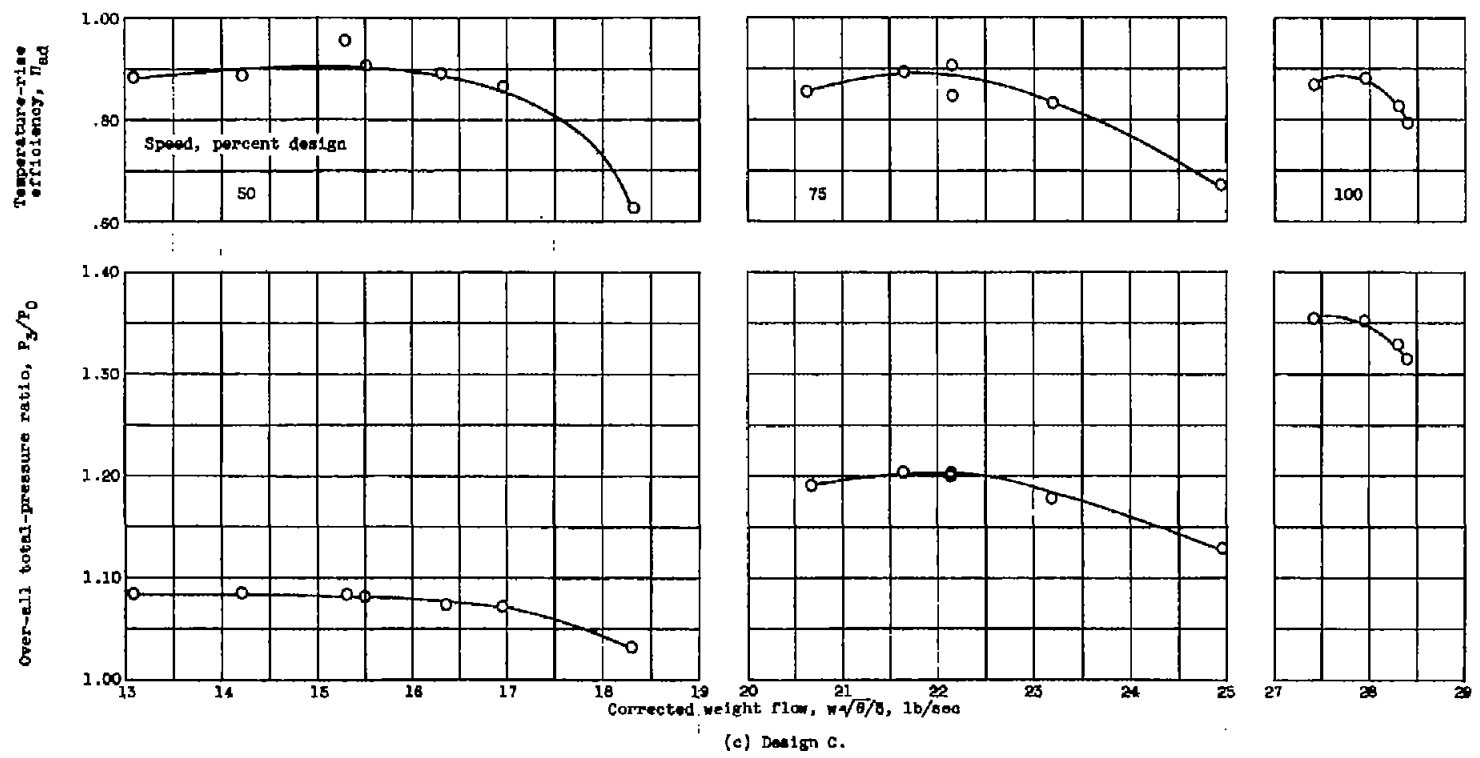
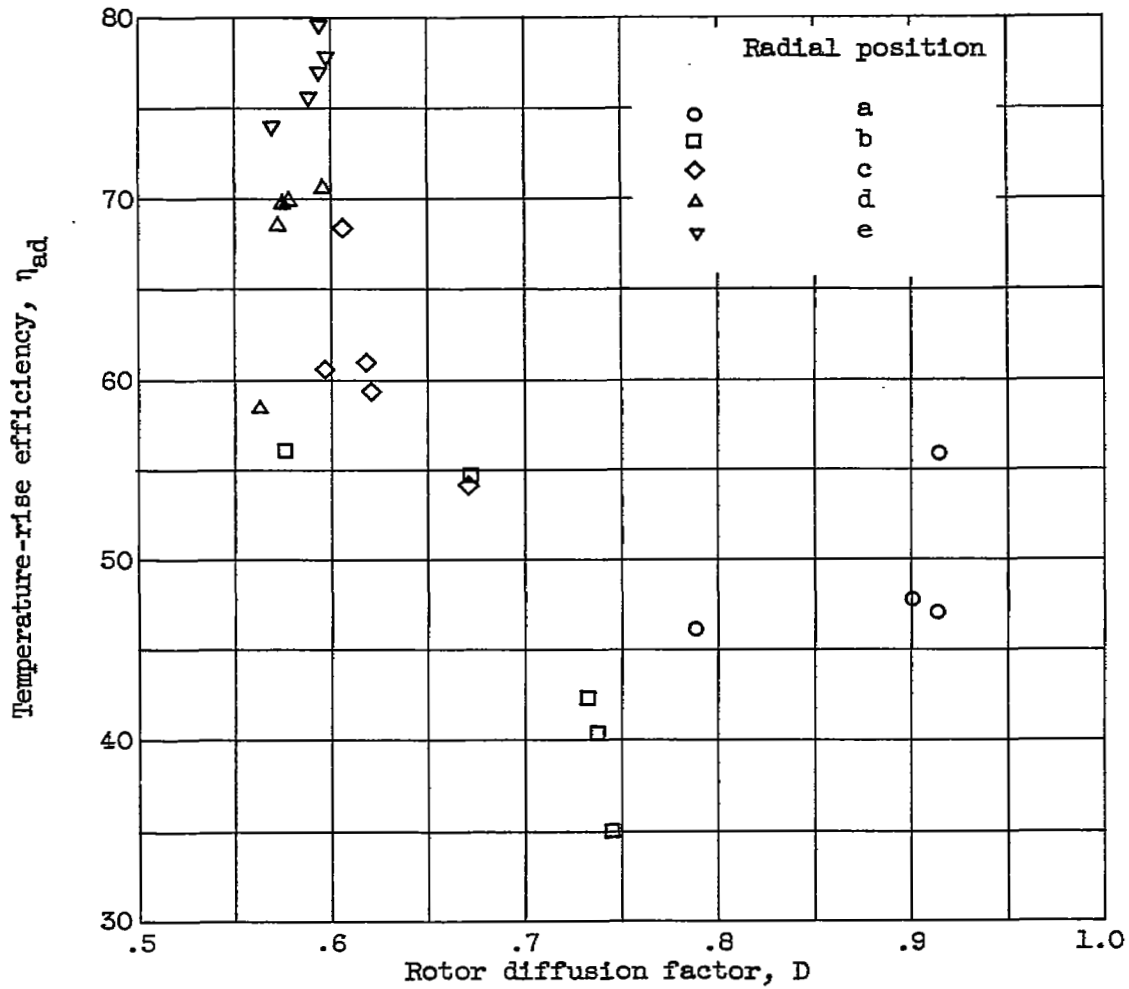


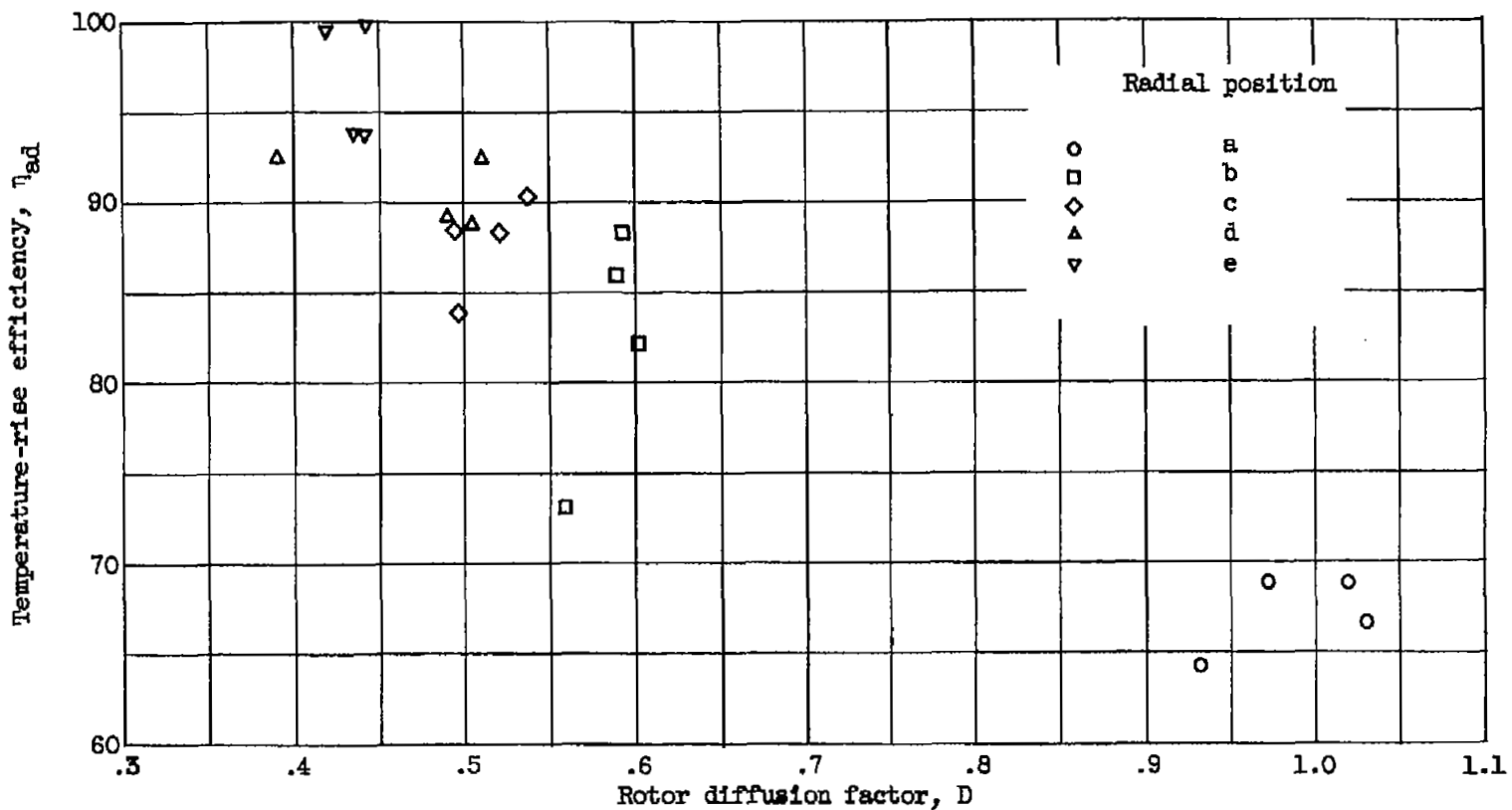
Figure 6. - Concluded. Variation of over-all total-pressure ratio and temperature-rise efficiency with corrected weight flow.

3335 \*  
CK-4 back



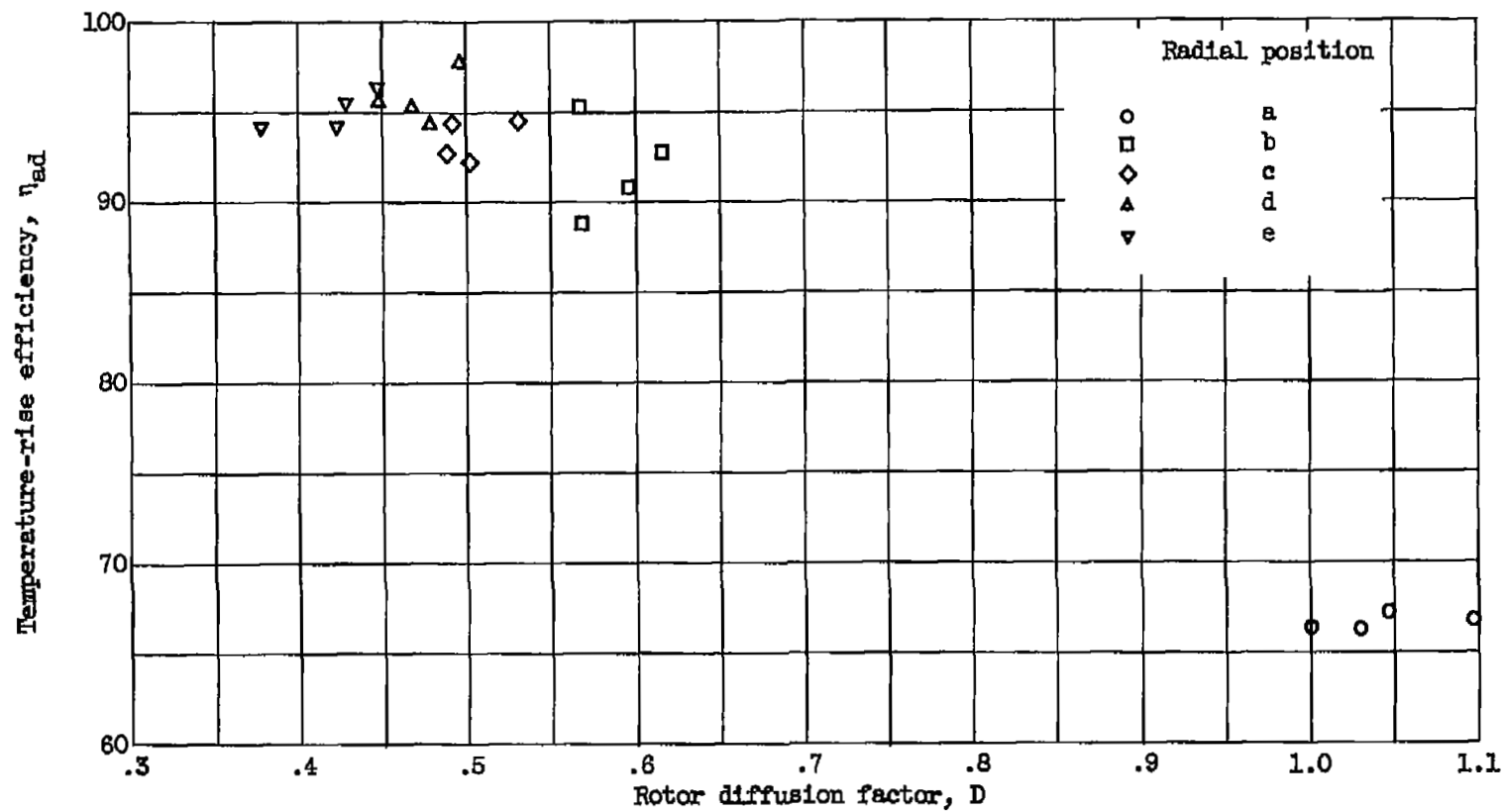
(a) Design A.

Figure 7. - Variation of rotor blade element efficiency with diffusion factor at design speed.



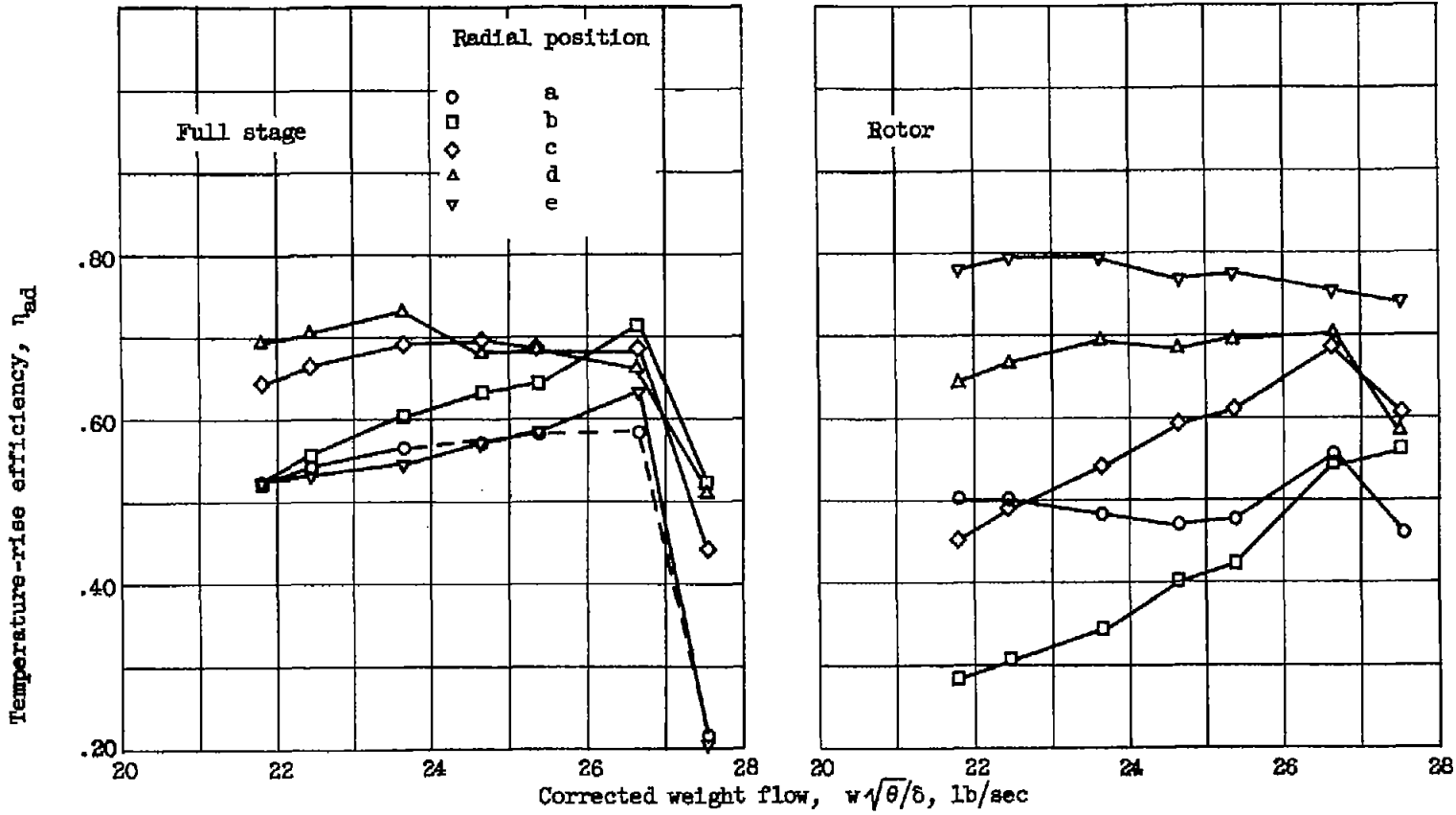
(b) Design B.

Figure 7. - Continued. Variation of rotor blade element efficiency with diffusion factor at design speed.



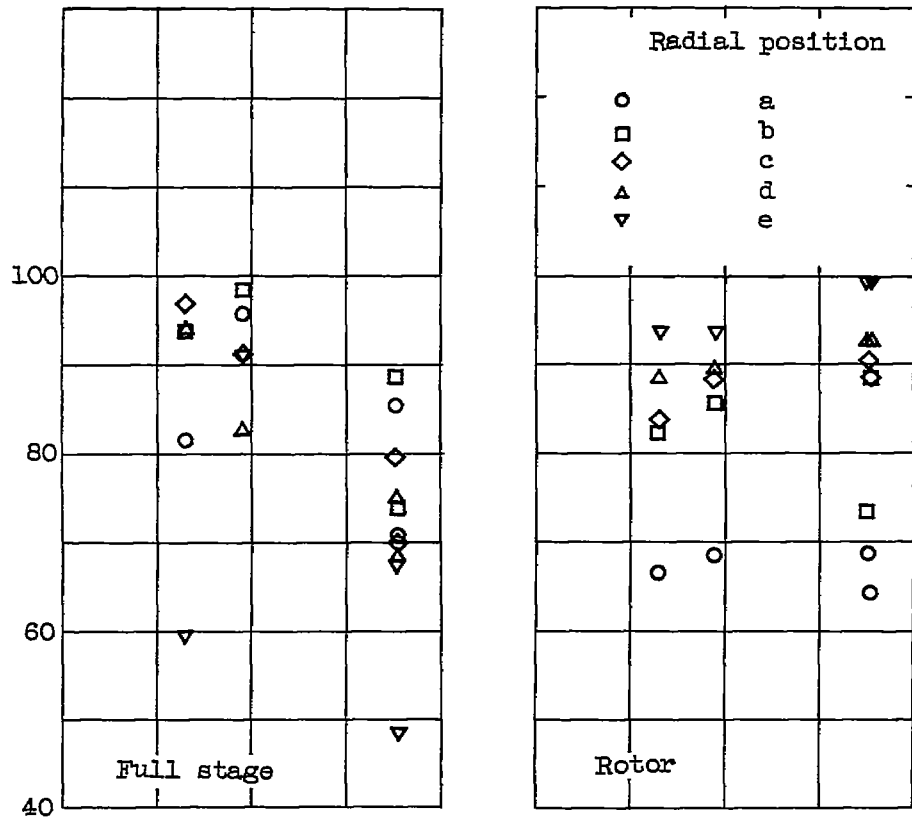
(c) Design C.

Figure 7. - Concluded. Variation of rotor blade element efficiency with diffusion factor at design speed.

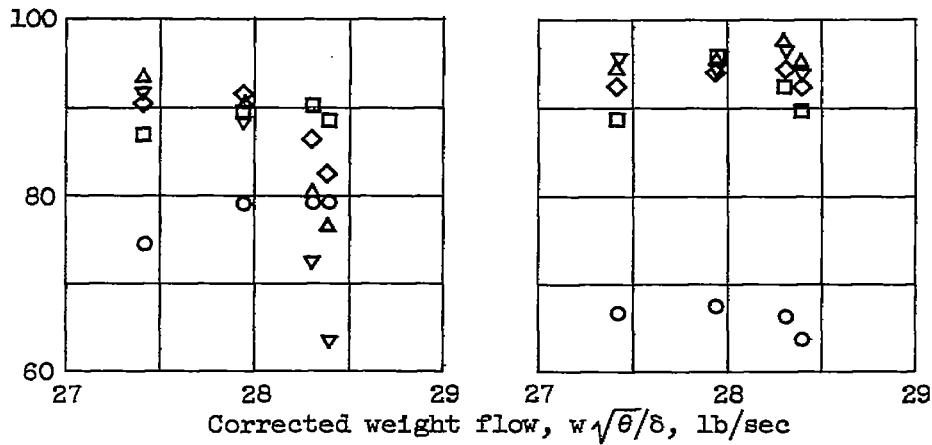


(a) Design A.

Figure 8. - Comparison of radial element efficiencies downstream of the rotor and stator at design speed.



(b) Design B.



(c) Design C.

Figure 8. - Concluded. Comparison of radial element efficiencies downstream of rotor and stator at design speed.

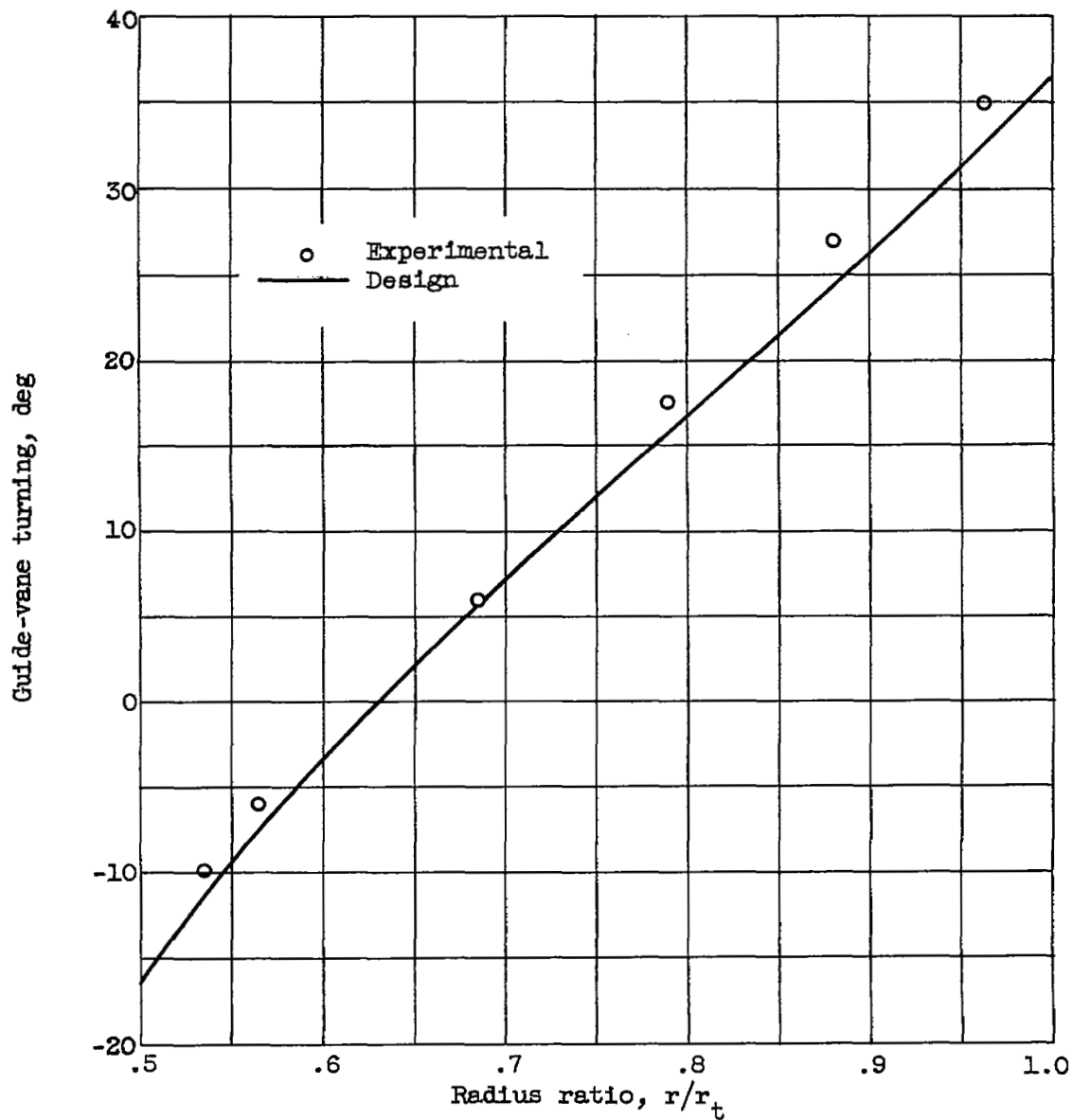


Figure 9. - Comparison of measured guide-vane turning with design values for design A.

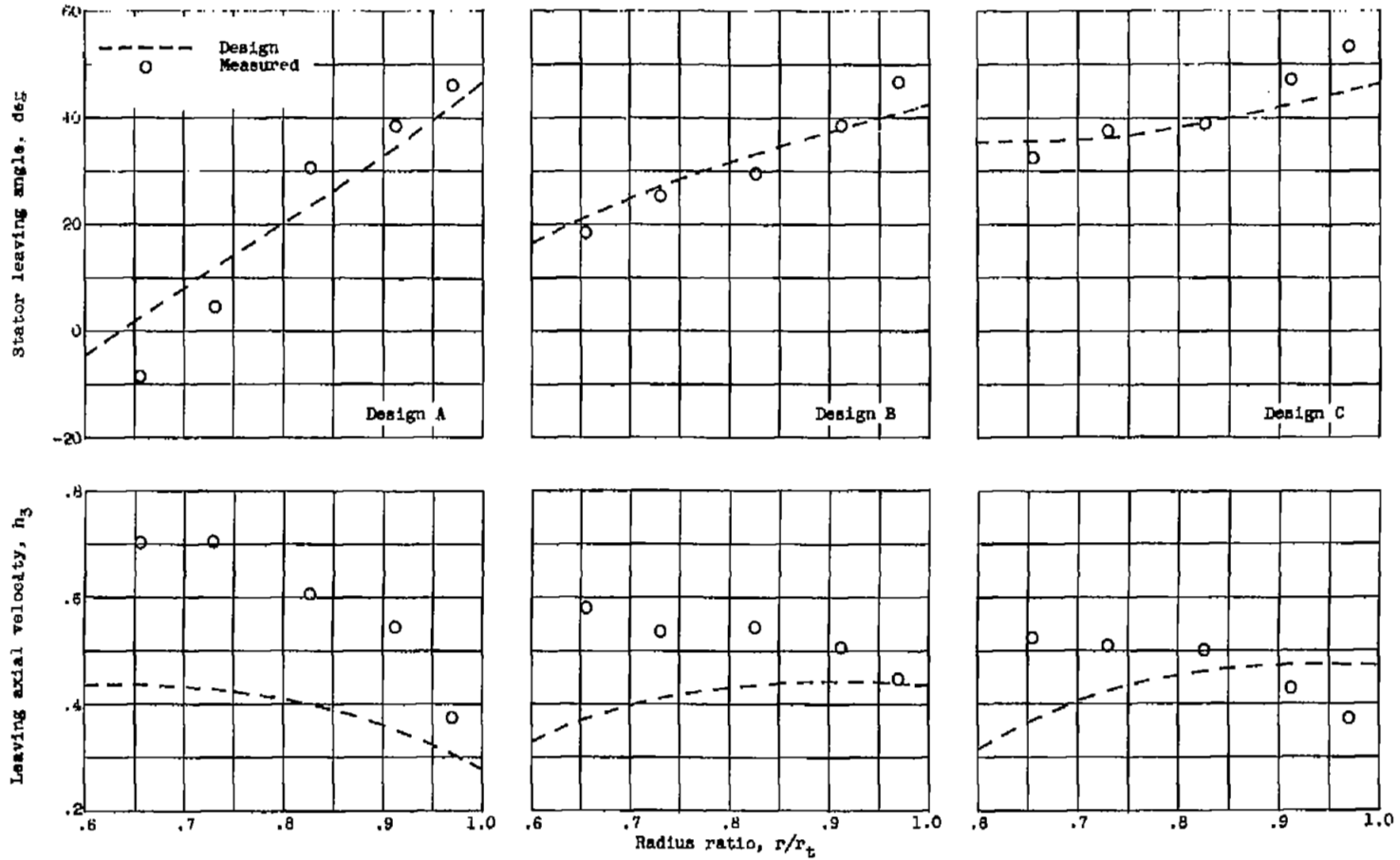


Figure 10. - Comparison of measured flow angles and axial velocities downstream of stators with design values for all three designs.

NASA Technical Library



3 1176 01435 4337

f  
t

f  
5

f  
t

